Solid-state multinuclear magnetic resonance investigation of Pyrex®

S. Prasad [a], Ted M. Clark [a], Travis H. Sefzik [a], Hyung-Tae Kwak [b],
Zhehong Gan [b], Philip J. Grandinetti [a],*

[a] *Department of Chemistry, The Ohio State University, 120 W. 18th Avenue, Columbus, OH 43210-1173, United States*
[b] *Center of Interdisciplinary Magnetic Resonance, National High Magnetic Field Laboratory, Tallahassee, FL 32310, United States*

Abstract

Pyrex® is an ubiquitous material that has attained widespread use in laboratory glassware and household utensils due to its properties, cost effectiveness, and ease of fabrication. Despite its importance, the structure of borosilicate glass such as Pyrex® is not fully understood. Here, we report high resolution ^{29}Si, ^{27}Al, and ^{11}B magic-angle spinning (MAS) nuclear magnetic resonance (NMR) spectroscopic measurements at 9.4 and 19.5 T, combined with ^{27}Al and ^{11}B multiple-quantum MAS (MQ-MAS), and ^{11}B Rotor Assisted Population Transfer (RAPT), to identify structural features in Pyrex®. A distribution of Q^4 silicon and aluminum sites is observed, and there is no evidence of five or six coordinated aluminum. The ^{27}Al quadrupolar coupling constants for the tetrahedral aluminum varied from 3.5 to 4.5 MHz, while the isotropic chemical shifts varied from 50 to 65 ppm. Boron-11 measurements resolve four distinct distributions in boron environments: two identified as tetrahedral, BO_4, and two as trigonal, BO_3. Tetrahedral sites are distinguished by different second coordination spheres, e.g., $BO_4(0\ B, 4\ Si)$ and $BO_4(1\ B, 3\ Si)$, and the trigonal sites based on the symmetry of the boron environments.
© 2006 Elsevier B.V. All rights reserved.

Keywords: Ab initio; Oxide glasses; Alkali silicates; Aluminosilicates; Borosilicates; Silicates; NMR, MAS-NMR and NQR; Short-range order

1. Introduction

Pyrex® is a borosilicate glass that has attained widespread commercial use. It can withstand temperature of 500 °C, has high mechanical strength, a 92% light transmittance at 2 mm thickness, and is resistant to strong alkalis and acids. Also, it is easily fabricated and economical. Despite its technological importance, there has, surprisingly, been only one solid-state NMR study of Pyrex®. In 1986, Turner et al. [1] used ^{11}B NMR to identify two-, four-coordinate and two three-coordinate boron sites in Pyrex® and were able to estimate the quadrupole coupling constant (C_q) values. In contrast, there have been ^{11}B NMR studies of numerous other borosilicate glasses, starting from 'wide line' solid-state NMR studies [2–4] and continuing to more recent work involving high resolution methods [5,6]. In these recent investigations, methods such as magic-angle spinning (MAS), dynamic-angle spinning (DAS) and multiple-quantum MAS (MQ-MAS) were used to identify BO_4 sites with two, three and four silicon neighbors and to obtain a more complete characterization of the distribution of quadrupole coupling constants (C_q), asymmetry parameter (η_q), and isotropic chemical shifts (δ_{iso}^{CS}) [5,7–14].

Here, we report a comprehensive NMR study of Pyrex® by examining the boron, silicon and aluminum environments. We also demonstrate the combined use of high field (19.5 T) MAS, lower field (9.4 T) Rotor Assisted Population Transfer (RAPT) [15–19] and MQ-MAS [20,21]. These sensitivity and resolution enhancement methods were used to extract NMR parameters.

2. Experimental methods

A commercial sample of Pyrex® was used for the investigation. The chemical composition (percentage by weight) of

---

Pyrex® glass, determined by wet chemical analysis is as follows: $SiO_2 = 80.6\%$; $B_2O_3 = 13.0\%$; $Na_2O = 4.0\%$; $Al_2O_3 = 2.3\%$; miscellaneous traces $= 0.1\%$, corresponding to mole fractions of 0.830, 0.116, 0.040, and 0.0140, respectively. This composition corresponds to $K = 7.18$ and $R = 0.35$, where K and R are the molar ratio of SiO_2 to B_2O_3 and Na_2O to B_2O_3, respectively. Additionally, since the glass composition contains aluminum, we define R' as $(Na_2O\text{-}Al_2O_3)/B_2O_3$ that equals 0.224 (as discussed in Section 3). Analysis of the sample by electron microscopy indicated no apparent phase separation.

Low field (9.4 T) MAS, RAPT and MQ-MAS and high field (19.5 T) MAS measurements were made using Bruker AVANCE spectrometers and 4 mm MAS probeheads with spinning rates of 10–12 kHz. To obtain the RAPT sensitivity enhancement in the [11]B spectra, frequency switched Gaussian pulses ($\sigma = 2.855\ \mu s$, $\tau_p = 15\ \mu s$) were applied at pre-determined frequency offsets [17–19]. A 2 μs delay between each pulse in the RAPT pulse train was used to allow time for the transmitter phase to stabilize. The recycle delay was 10 s. The number of Gaussian pulses used in the RAPT preparation was 16 or 40 when using rf field strengths of 100 kHz or 40 kHz, respectively. The shifted-echo method [22] was used for acquiring and processing triple quantum RIACT data [23]. Radiofrequency field strengths of 140 kHz for the quarter rotor period spin-locking pulse and 40 kHz for the $\pi/2$ pulse were used. All RIACT experiments were performed using 5 s recycle delay. There were 32 t_1 points acquired with an increment of 30 μs. Since the offset dependence is large for sites having larger quadrupolar frequencies, the spin-locking field was set at the center of the line shape arising from the BO_3 resonance. The T_1 times measured using saturation recovery method were of the order of 2.5 s for both the resonances. Silicon-29 MAS NMR spectrum was measured using a relaxation delay of 100 s. For the [27]Al MQ-MAS spectrum, 50 hypercomplex points with 24 μs increment were acquired. 1 M H_3BO_3 solution (19.6 ppm), Tetramethyl silane (0.0 ppm) and 1 M $Al(NO_3)_3$ solution (0.0 ppm) were used to calibrate the radiofrequency field and as chemical shift references.

3. Results and discussion

3.1. ^{29}Si NMR spectra

Silicon-29 MAS NMR can often resolve resonances from five different types of silicate tetrahedra having varying numbers (n) of bridging oxygen, commonly described as $Q^{(n)}$ species [24]. Systematic variations of [29]Si chemical shifts with structure occur, with the [29]Si chemical shift becoming increasingly negative as the number of bridging oxygen linkages increases. This occurs due to a greater degree of electronic shielding of the central Si-atom. Tetrahedral Q^4 [29]Si chemical shift values generally range from -102 to -116 ppm when the next nearest neighbor atoms are silicon [24–26]. The [29]Si chemical shift values for Q^3

Si-atoms range from -88 to -101 ppm when the bridging oxygen are present in Si–O–Si linkages, although it should be noted that such environments including non-bridging oxygen atoms are not expected in the composition range of Pyrex®. If the next nearest neighbor atoms are not silicon, however, different chemical shift ranges are observed. For example, a Q^4 silicon in which one of the bridging oxygen atom is in a Si–O–Al linkage is described by chemical shift values from -97 to -107 ppm, and a Q^4 silicon with two aluminum neighbors has values from -92 to -100 ppm. The [29]Si chemical shift values for Q^4 sites with boron next nearest neighbors are expected to be similar to those reported for silicates with aluminum next nearest neighbors; boron and aluminum are both Group IIIA elements and a strong correlation has been shown between group electronegativity and the [29]Si chemical shift [25].

In Fig. 1 the ^{29}Si NMR spectrum at 9.4 T of Pyrex® is shown, which consists of a broad resonance centered at -107 ppm, and a smaller resonance ($\leqslant 5\%$) at -92 ppm. Based on these chemical shift values, the major contribution to the resonance centered at -107 ppm is identified as Q^4 Si-atoms. The broad range of chemical shift values is due to variations in the neighboring bridging oxygen angles, inter alia. It is possible, however, that the next nearest neighbor atoms are not exclusively other Si-atoms, but perhaps other network forming cations, i.e., boron and aluminum. The contribution from each of these other sites are expected to overlap near -100 to -104 ppm.

In addition to the major resonance attributed to Q^4 Si-atoms with four Si–O–Si linkages, or three Si–O–Si linkages and either a Si–O–B or Si–O–Al linkage, a minor resonance is present near -92 ppm. When assigning this resonance it is useful to note that non-bridging oxygen atoms are not expected in sodium borosilicate or aluminosilicate glasses with low Na_2O content. Recent ^{11}B and ^{17}O MQMAS NMR experiments provide clear evidence of the exclusive presence of Q^4 species at small R regions [5]. Therefore, instead of assigning the -92 ppm component to Q^3 species, it appears more plausible to identify this feature as a Q^4 species associated with abundant non-Si neighbors in the second coordination, such as BO_4 units. There have been several ^{29}Si NMR studies in which a similar low frequency peak has been observed. Nanba et al. [27] studied borosilicate glasses with varying amount of Na_2O ($R = 0\text{–}1.2$) by ^{11}B and ^{29}Si NMR. In this work the authors identify a [29]Si resonance near -90 ppm, but caution against attributing this component to Q^3 species for glasses with negligible non-bridging oxygen atoms. Silicon-29 chemical shift values for minerals such as olenite [28] and danburite [29], which contain Si–O–B linkages, have also been reported and are typically between -85 and -90 ppm. These other investigations support the assignment of the shoulder at -92 ppm in the ^{29}Si NMR spectrum of Pyrex to the presence of Si–O–B or Si–O–Al linkages, perhaps resulting in Q^4 silicon environments with two non-Si–O–Si linkages.
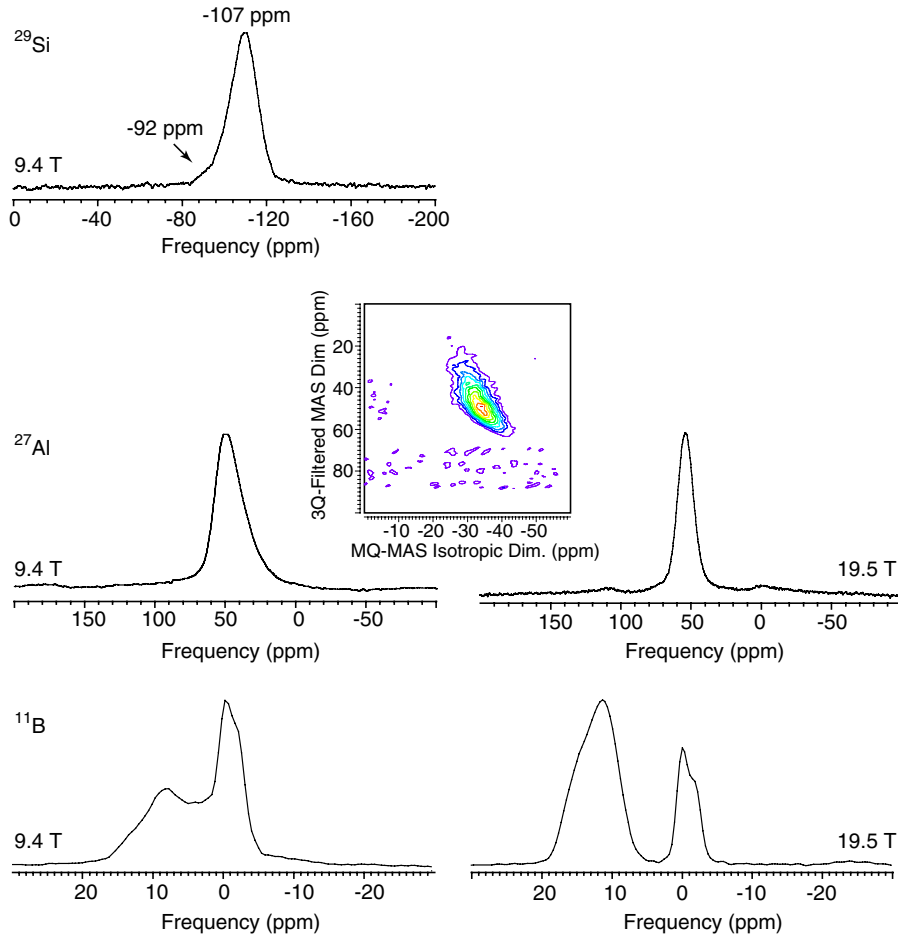
Fig. 1. From top to bottom are the ^{29}Si, ^{27}Al, and ^{11}B MAS NMR spectra of Pyrex$^®$ obtained at 9.4 T and at 19.5 T for ^{27}Al, and ^{11}B. Also shown is the ^{27}Al MQ-MAS spectrum obtained at 9.4 T.

3.2. ^{27}Al NMR spectra

For odd-half integer quadrupolar nuclei (like ^{27}Al, ^{11}B), the observed total frequency shifts in the MAS spectra (δ_{iso}^{Total}) are directly related to the isotropic chemical shifts (δ_{iso}^{CS}) and isotropic second-order quadrupolar shifts (δ_{iso}^{2Q}) by:

$$\delta_{iso}^{Total} = \delta_{iso}^{CS} + \delta_{iso}^{2Q}. \tag{1}$$

The second-order isotropic shift is a function of the quadrupolar product (P_q), the Larmor frequency (ν_L) and the spin quantum number (I).

$$\delta_{iso}^{2Q} = \frac{-3[I(I+1) - 3/4]}{40\nu_L^2 I^2 (2I-1)^2} P_q^2 \times 10^6 \text{ (ppm)}, \tag{2}$$

where the quadrupolar product (P_q) is related to the quadrupolar coupling constant (C_q), which in turn is related to the quadrupolar frequency (ν_q) as

$$P_q = C_q \sqrt{1 + \frac{\eta_q^2}{3}}, \tag{3}$$

$$C_q = \frac{e^2 qQ}{h}, \tag{4}$$

$$\nu_q = \frac{3Cq}{2I(2I-1)}. \tag{5}$$

It has been reported that in the case of aluminoborates and aluminosilicates, aluminum may occur in four-, five-, and six-coordination with oxygen nearest neighbors. These different coordination environments have quite different ^{27}Al shifts (δ_{iso}^{Total}). Four coordinate Al–O environments have ^{27}Al total shift values between 50 and 80 ppm (with respect to $Al(H_2O)_6^{3+}$), and those for five and six coordinate aluminum are 30–40 ppm and −10 to 15 ppm, respectively [24]. In aluminosilicates, tetrahedral aluminum with four silicon next nearest neighbors have a total shift range between 50 and 68 ppm.

In Fig. 1 we show the ^{27}Al NMR MAS spectrum of Pyrex$^®$ at 9.4 and 19.5 T, and the corresponding NMR parameters are given in Table 1. Unlike results reported for aluminoborates [30–32], the ^{27}Al NMR spectrum of Pyrex$^®$ at 9.4 T indicates solely the presence of four coordinated aluminum. Although there is distinct tailing in the line shape, even in the MQ-MAS spectrum (Fig. 1 inset), there is no indication of five-coordinated sites. The MAS NMR line shape reported here for spectra collected at 9.4 T is typical of distributions of C_q and isotropic chemical shift values (δ_{iso}^{CS}), and is commonly observed in aluminosilicate glasses [33].

Table 1
^{29}Si, ^{27}Al and ^{11}B NMR parameters for Pyrex®

Nucleus	Site identification	δ_{iso}^{CS} (± 0.2 ppm)	C_q (± 0.05 MHz)	η_q (± 0.05)	Relative intensity (± 2)
^{29}Si	Q^4	−107	n/a	n/a	95
^{29}Si	Q^4 with 2 non-Si neighbors	−92	n/a	n/a	5
^{27}Al	Q^4	54[a]	3.5–4.5	n/a	100
^{11}B	BO_4 (0B, 4Si)	−1.0 (0.2)	0.3 (0.5)	0	10
^{11}B	BO_4 (1B, 3Si)	0.4 (1.2)	0.3 (0.5)	0	10
^{11}B	$BO_{3symmetric}$ (ring)	16.8 (16.0)	2.2 (2.3)	0.2	40
^{11}B	$BO_{3asymmetric}$ (see text)	12.7 (12.6)	2.65 (2.5)	0.8	40

δ_{iso}^{CS} is the isotropic chemical shift, C_q, the quadrupolar coupling constant, and η_q, the asymmetry parameter. The numbers in parentheses are from Turner et al. [1].

[a] Denotes (δ_{iso}^{Total}). The above values reflect a distribution rather than a margin of error.

Analysis of the MQ-MAS data confirms a distribution of local aluminum environments. The C_q varied from 3.5 to 4.5 MHz, while the isotropic chemical shifts (δ_{iso}^{CS}) varied from 50 to 65 ppm. However, an average quadrupolar product (P_q) of 4 MHz was obtained by the analysis of the MQ-MAS data. C_q values in this range are consistent with aluminum atoms being present in polyhedra that are not severely strained, i.e., there are minimal distortions in tetrahedral bond lengths and bond angles [24]. This finding is consistent with AlO_4 tetrahedra being predominantly connected to four neighboring SiO_4 tetrahedra [33]. ^{27}Al MAS spectrum acquired at 19.5 T shows a major resonance with (δ_{iso}^{Total}) of 54 ppm Fig. 1. Significant line narrowing is noticeable, and again five- or six-coordinated aluminum are not observed above the limit of detection.

When discussing the assignment of the aluminum resonance in Pyrex®, it is useful to consider the aluminum environments expected in a sodium borosilicate glass with a small concentration of aluminum.

With the addition of Na_2O, O^{2-} ions are introduced into the glass network. With respect to the network former oxides B_2O_3 and Al_2O_3, the following reactions occur as the Na_2O concentration increases [31,34]:
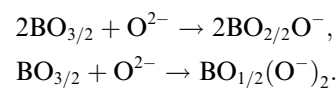
(A) Conversion of octahedral aluminum to tetrahedral aluminum,

$$2AlO_{6/2} + O^{2-} \rightarrow 2AlO_{4/2}^-,$$
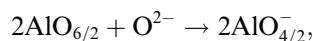
(B) conversion of three-coordinate boron to tetrahedral $BO_{4/2}^-$ units,

$$2BO_{3/2} + O^{2-} \rightarrow 2BO_{4/2}^-,$$
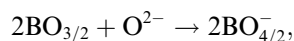
(C) formation of three coordinate boron having one or two non-bridging oxygen,

$$2BO_{3/2} + O^{2-} \rightarrow 2BO_{2/2}O^-,$$
$$BO_{3/2} + O^{2-} \rightarrow BO_{1/2}(O^-)_2.$$

These reactions (A)–(C) are closely dependent on the composition of the glass. For a sample with a low aluminum content and also a low alkali content like Pyrex® ($R = 0.35$), reaction (A) is expected to go to completion and so aluminum will be in tetrahedral environments. This suggestion is consistent with the results discussed here for Pyrex®. Also, based on the composition of this sample, reaction (B) is expected to dominate over reaction (C).

The species potentially bonded to a given aluminum atom will include $SiO_{4/2}$ tetrahedra, boron species including $BO_{3/2}$, $BO_{4/2}^-$, and trigonal boron sites with one or two non-bridging oxygen. Although numerous boron species are potential neighbors, a statistical distribution of different types of boron neighbors is not expected. Specifically, based on charge valence arguments and recent experimental results, it is likely that negatively charged species, e.g., $AlO_{4/2}^-$ or $BO_{4/2}^-$, will be under-represented as aluminum neighbors [34]. Finally, in Pyrex®, Na-cations will be near $AlO_{4/2}^-$ tetrahedra since charge-balancing cations are not randomly distributed, but rather are associated with more negatively charged oxygen sites [33].

Based on the stoichiometry of the glass, silicon species are, of course, the most probable neighbors for aluminum [33]. The aluminum resonance with $\delta_{iso}^{Total} = 54$ ppm at 19.5 T is therefore expected to be tetrahedral aluminum with silicon species as neighbors. This assignment is consistent with several other NMR investigations of aluminum in sodium aluminosilicates or borosilicates [35,36].

Finally, since Na ions serve as charge compensating cations for the $AlO_{4/2}^-$ sites, it is useful here to describe a ratio R' as $(Na_2O–Al_2O_3)/B_2O_3$. Unlike a sodium borate system in which a modifier concentration is crucial for describing boron coordination, in Pyrex® the Na modifiers must also act as charge-compensating cations near aluminum tetrahedra leading to an overall reduction in R (Na_2O/B_2O_3). In Pyrex®, for example, R' is 0.224, representing a significant decrease from an R value of 0.35.

3.3. ^{11}B NMR spectra

There have been several recent reports of ^{11}B MAS NMR spectroscopic studies on borates and borosilicates [5,7–14]. These studies have shown that the BO_4 sites have negligible second-order quadrupolar broadening with C_q values of 0.3 MHz and η_q values of 0, and have isotropic chemical shifts in the range of 1.5 to −2.5 ppm. These sites are bonded either to 2, 3, or 4 other boron atoms consisting of B–O–B or B–O–Si linkages. In contrast, the BO_3 sites

have much larger C_q values of 2–2.5 MHz with η_q varying from 0 to 1 depending on the number of non-bridging oxygen. The isotropic shifts fall in the range of 12–18 ppm.

The [11]B MAS spectrum in Fig. 1 of Pyrex® at 9.4 T shows a narrow resonance centered at −0.1 ppm and a broad resonance centered near 8.2 ppm. The narrow resonance had spinning sidebands arising from the satellite transitions extending up to 150 kHz in the single pulse spectrum (not shown). Thus, the narrow resonance is dominated by expected resonances from BO_4 groups with C_q values near 0.3 MHz. The broad resonance is assigned to those expected for BO_3 sites, which have much larger C_q values. While complete resolution of BO_4 and BO_3 sites is not achieved at 9.4 T, these two environments are well resolved at 19.5 T into two resonances, one centered at −1 ppm.

Fig. 2 shows the [11]B RIACT spectrum of Pyrex®. The broad resonance in the MAS spectrum (Fig. 1 (bottom)) now is separated into two BO_3 sites in the isotropic dimension and the narrow resonance now comprises exclusively of BO_4 sites. From the MAS dimension, it appears that the narrow BO_4 resonance has contributions from the BO_3 resonances in the MAS spectrum (Fig. 1). The slight slant in the 2D spectrum even after the shearing transformation indicates a small distribution of both quadrupolar frequencies and isotropic shifts, the latter dominating for the BO_4 resonance.

The RAPT method, which enhances the central transition intensity, can also be used to determine the quadrupolar coupling constant [17]. This is achieved by plotting the enhancement factor as a function of offset frequencies (i.e., the RAPT profile). By measuring the offset frequency where there is no apparent enhancement (ν_{edge}), the quadrupolar coupling constant can be determined. Fig. 3 shows the measured RAPT MAS profiles for the broad resonance with two different rf power levels. When the samples contained multiple resonances, the enhancement was calculated using intensities measured from the Fourier transformed spectra, and not from the echo top intensity. For the broad
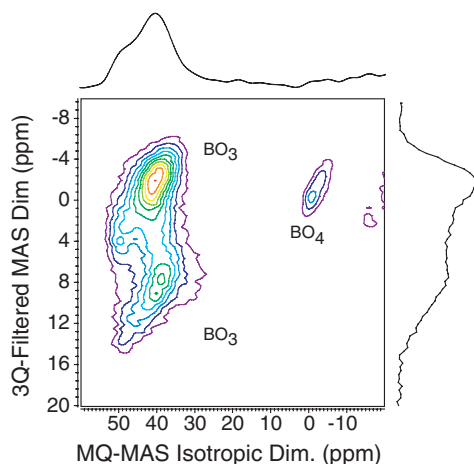

(a)

(b)
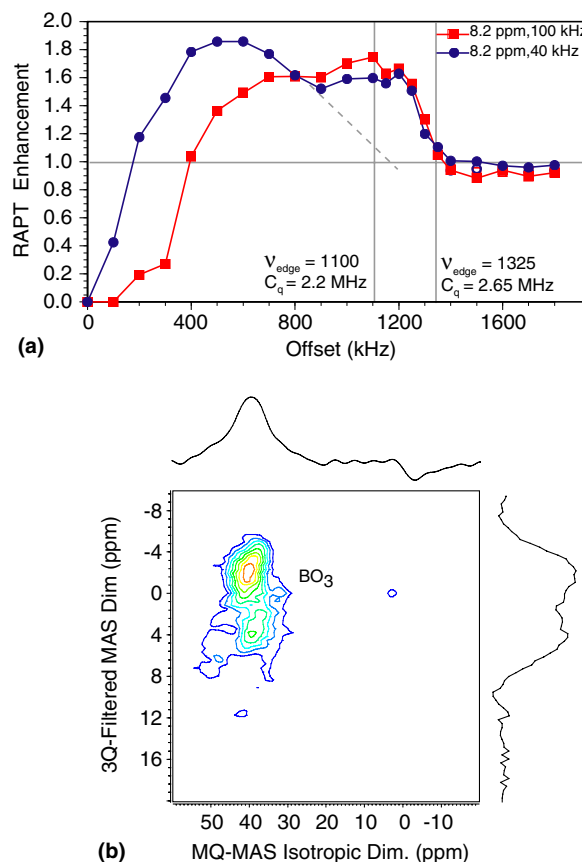
Fig. 3. (a) The measured [11]B RAPT MAS enhancement factor as a function of frequency offsets at two different rf-power levels. Vertical lines indicate ν_{edge} values. (b) $\pi/2$-RAPT-RIACT spectrum of Pyrex®. The RAPT offset frequency was 1300 kHz.

resonance, enhancement factor of 1.7 can be achieved at an offset frequency of 900 kHz by using high power Gaussian pulses; with lower power, enhancement factor of 1.9 can be achieved at offset frequencies of 500–600 kHz. At both power levels, the enhancement factor drops to 1 near 1.4 MHz with a ν_{edge} of 1.325 MHz, and hence a C_q of 2.65 MHz. The rapid loss of the enhancement factor at offsets greater than 1 MHz suggests high η_q value as well. The RAPT profile at lower power level shows a distinct enhancement at 500 kHz and another one at 900 kHz, the latter enhancement similar to the one observed at high power. Thus, these profiles are indicative of two different resonances (one with a C_q of 2.65 MHz and the other one with a lower C_q value) contributing to the signal intensity of the broad peak. Since the C_q value of the BO_4 sites is estimated to be 0.3 MHz, the RAPT offset frequency for applying the Gaussian-shaped pulses is too close to the central transition and no signal enhancement is expected. Thus, the underlying component in the RAPT profile of the BO_3 resonance has a C_q of 2.2 MHz. These values are comparable to those reported by Turner et al. [1].

Unlike the MQ-MAS methods [20,21] where the quadrupolar product P_q is usually determined, the RAPT method provides a direct measure of the C_q values. P_q is

Fig. 2. [11]B 3Q RIACT spectrum of Pyrex® at 9.4 T.

related to C_q by Eq. (3), where C_q is the quadrupolar coupling constant and η_q the asymmetry parameter. By the judicious comparison of the results obtained by these two methods, both C_q and η_q can be determined.

Previously, we had demonstrated that, while a RAPT preparation can be used to enhance the signal intensity in the RIACT experiment [16], a modified RAPT scheme (π/2-RAPT) can be easily implemented to eliminate contributions from sites having smaller quadrupolar frequencies [18]. In this method, the initial $\pi/2$ pulse presaturates the central transition of all the sites and the magnetization of the larger C_q sites are revived using the RAPT pulse train at desired offset frequencies [18]. In the case of Pyrex®, the 'window' to employ such a scheme to eliminate the BO$_4$ sites as well as the BO$_3$ site with smaller C_q of 2.2 MHz is narrow (BO$_3$ site with a C_q of 2.65 MHz is one of the BO$_3$ sites, see Fig. 3(a)). Since the central transition nutation rates are much larger for the BO$_4$ sites, length of the initial $\pi/2$ pulse was chosen to suppress the BO$_4$ sites as well as the BO$_3$ site with smaller coupling, causing some dispersive components in the resulting 2D spectrum. Fig. 3(b) shows the π/2-RAPT-RIACT spectrum acquired with a RAPT offset frequency of 1300 kHz. The contributions from BO$_4$ sites and the BO$_3$ site with smaller coupling ($C_q = 2.2$ MHz) are completely eliminated. Moreover, it is apparent that the sites having larger coupling has a distribution of quadrupolar coupling constants ($C_q = 2.65 \pm 0.05$ MHz). From the position of the resonances in the MAS and the isotropic dimensions, the quadrupolar product (P_q) and isotropic shifts (δ_{iso}^{CS}) have been calculated and are listed in the Table 1. The η_q values were obtained by substituting the C_q values determined from the RAPT experiments.

3.4. Boron assignments

Boron-11 NMR measurements resolve four distinct boron environments (Fig. 4), and the NMR parameters for these sites (Table 1) are in good general agreement with values reported by Turner et al. [1]. As we have discussed, the two resonances with chemical shift values of -1.0 and 0.4 ppm are assigned to tetrahedral boron atoms. The small C_q (near 0.3 MHz) and small η_q (near 0) values for these resonances support this assignment. The recent systematic investigation of sodium borosilicate glasses has established that a slight upfield shift in chemical shift occurs for Q^4 boron atoms with three silicon neighbors with respect to boron atoms with four silicon neighbors [5]. It is therefore likely that the resonance observed in Pyrex® with a chemical shift of 0.4 ppm arises from a Q^4 B (3 Si, 1 B) site, and the resonance at -1.0 ppm is a Q^4 B (4 Si) site.

For the two BO$_3$ resonances, the assignment of the one having lower C_q (2.2 MHz) and η_q (0.2) values is straightforward. It has been well documented [5,7–14] that symmetric BO$_3$ sites (BO$_{3S}$) having zero or 3 non-bridging oxygen exhibit low η_q value (0–0.2). A recent report [5]

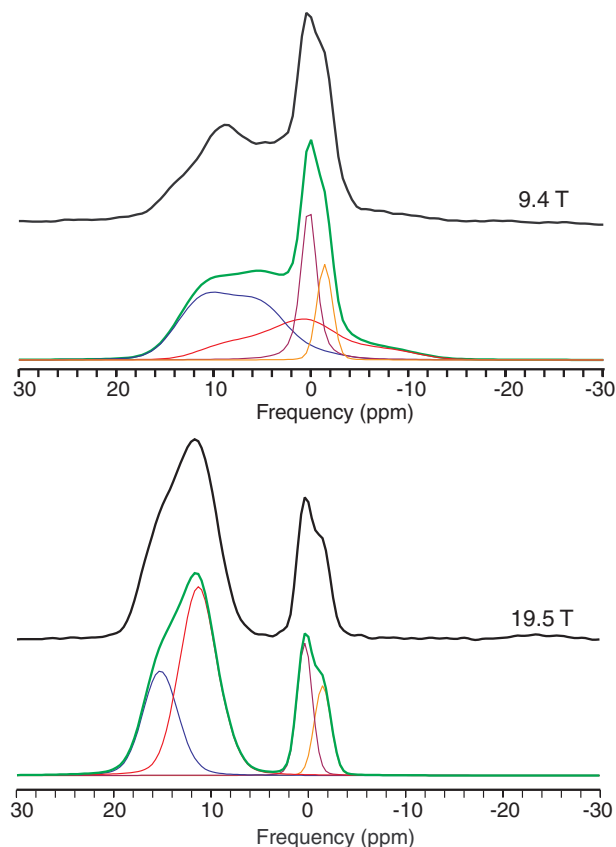Fig. 4. ^{11}B MAS NMR spectrum of Pyrex®. The black lines are the experimental spectra. The green lines represent the spectra fit to simulated line shapes using the parameters derived from RAPT and RIACT data. The individual components are also shown. (For interpretation of the references in color in this figure legend, the reader is referred to the web version of this article.)

has suggested that the BO$_{3S}$ sites can be further classified into BO$_{3(ring)}$ and BO$_{3(non-ring)}$ sites with isotropic shifts of 17 ppm and 13 ppm, respectively. Thus, the BO$_{3S}$ sites in Pyrex®, which have an isotropic chemical shift of 16.8 ppm, are present predominantly in ring structures.

The remaining BO$_3$ resonance has a smaller isotropic chemical shift near 12.8 ppm. This value is consistent with previous studies which have examined the relationship between δ_{iso}^{CS}(BO$_3$) and the silica content for binary B$_2$O$_3$ or ternary borosilicate glasses [7,24]. As the SiO$_2$ content increases, the δ_{iso}^{CS}(BO$_3$) generally decreases, a trend taken to indicate that the three-coordinate boron is mixing with the silica network. This is consistent with the assignment of the 12.8 ppm boron resonance to a non-ring boron environment in Pyrex®.

The 12.8 ppm BO$_3$ resonance also has relatively larger C_q (2.65 MHz) and η_q (0.8) values. The presence of BO$_3$ resonances with larger C_q and η_q, i.e., greater than 2.5 MHz and 0.5, respectively, are infrequently reported for borate glasses. Trigonal boron with higher C_q and η_q values have been observed in calcium metaborate (CaO · B$_2$O$_3$) [37] and also for boron impurities in calcite (CaCO$_3$) [38]. There are also reports [12,34] of such species in crystalline and glassy borates where the concentration of Na$_2$O dictates

their formation; higher concentration results in the formation of BO_3 species that have 1 or 2 non-bridging oxygen, and the presence of asymmetric BO_3 species complementing the formation of Q^3 silicon. However, the assignment of the second BO_3 resonance in Pyrex® to asymmetric BO_3 species requires caution. The chemical composition of Pyrex® indicates that it contains 3.8% of Na_2O. According to the model proposed by Dell et al. [4], it seems rather unlikely that asymmetric BO_3 would form in Pyrex® given its low Na_2O concentration ($R = 0.35$). Indeed, since some of the Na cations are expected to be near aluminum tetrahedra, relatively little Na_2O ($R' = 0.224$) is available for the formation of asymmetric BO_3 environments. As discussed earlier, the conversion of three-coordinate boron to tetrahedral boron units is expected to dominate over the formation of boron having non-bridging oxygen neighbors. At present, therefore, a definitive description that accounts for the unexpectedly high η_q of the 12.8 ppm BO_3 resonance is not possible. Further work is needed, perhaps involving a combination of RAPT and MQ-MAS experiments to systematically determine the quadrupole coupling parameters for borosilicate glasses with compositions analogous to Pyrex®.

4. Conclusion

We have reported a comprehensive NMR study (^{11}B, ^{27}Al and ^{29}Si) of the commonly used glass Pyrex®. High field (19.5 T) NMR measurements and sensitivity enhancement technique like RAPT provided valuable information regarding the structural complexity of the glass. ^{11}B NMR spectra showed multiple BO_4 sites, a symmetric BO_3 site with boron occupying ring structure and an asymmetric BO_3 site. Aluminum is present exclusively in tetrahedral environments. Silicon occurs predominantly as Q^4, with a minor amount of Q^4 silicon with aluminum or boron neighbors. It is noteworthy that RAPT and MQ-MAS are being combined to investigate glass structure even when peaks are overlapping at a relatively low field of 9.4 T.

Acknowledgements

References

[1] G.L. Turner, K. Smith, R.J. Kirkpatrick, E. Oldfield, J. Magn. Reson. 67 (1986) 544.

[2] P.J. Bray, Inorg. Chim. Acta 289 (1–2) (1999) 158.

[3] J. Zhong, P.J. Bray, J. Non-Cryst. Solids 84 (1–3) (1986) 17.

[4] W.J. Dell, P.J. Bray, S.Z. Xiao, J. Non-Cryst. Solids 58 (1) (1983) 1.

[5] L.S. Du, J.F. Stebbins, J. Phys. Chem. B 107 (37) (2003) 10063.

[6] S.K. Lee, C.B. Musgrave, P. Zhao, J.F. Stebbins, J. Phys. Chem. B 105 (2001) 12583.

[7] R. Martens, W. Muller-Warmuth, J. Non-Cryst. Solids 265 (1–2) (2000) 167.

[8] R.E. Youngman, J.W. Zwanziger, J. Am. Chem. Soc. 117 (4) (1995) 1397.

[9] R.E. Youngman, J.W. Zwanziger, J. Phys. Chem. 100 (41) (1996) 16720.

[10] S. Sen, Z. Xu, J.F. Stebbins, J. Non-Cryst. Solids 226 (1–2) (1998) 29.

[11] T. Yazawa, K. Kuraoka, T. Akai, N. Umesaki, W.F. Du, J. Phys. Chem. B 104 (9) (2000) 2109.

[12] J.F. Stebbins, P.D. Zhao, S. Kroeker, Solid State Nucl. Magn. Reson. 16 (1–2) (2000) 9.

[13] S. Kroeker, J.F. Stebbins, Inorg. Chem. 40 (24) (2001) 6239.

[14] S.K. Lee, J.F. Stebbins, Geochim. Cosmochim. Acta 66 (2) (2002) 303.

[15] Z. Yao, H.T. Kwak, D. Sakellariou, L. Emsley, P.J. Grandinetti, Chem. Phys. Lett. 327 (1–2) (2000) 85.

[16] H.T. Kwak, S. Prasad, Z. Yao, P.J. Grandinetti, J.R. Sachleben, L. Emsley, J. Magn. Reson. 150 (1) (2001) 71.

[17] S. Prasad, H.T. Kwak, T. Clark, P.J. Grandinetti, J. Am. Chem. Soc. 124 (18) (2002) 4964.

[18] H.T. Kwak, S. Prasad, T. Clark, P.J. Grandinetti, J. Magn. Reson. 160 (2) (2003) 107.

[19] H.T. Kwak, S. Prasad, T. Clark, P.J. Grandinetti, Solid State Nucl. Magn. Reson. 24 (2–3) (2003) 71.

[20] L. Frydman, J.S. Harwood, J. Am. Chem. Soc. 117 (1995) 5367.

[21] D. Massiot, B. Touzo, D. Trumeau, J.P. Coutures, J. Virlet, P. Florian, P.J. Grandinetti, Solid State Nucl. Magn. Reson. 6 (1) (1996) 73.

[22] P.J. Grandinetti, J.H. Baltisberger, A. Llor, Y.K. Lee, U. Werner, M.A. Eastman, A. Pines, J. Magn. Reson. Ser. A 103 (1) (1993) 72.

[23] G. Wu, D. Rovnyak, R.G. Griffin, J. Am. Chem. Soc. 118 (1996) 9326.

[24] K.J.D. Mackenzie, M.E. Smith, Multinuclear Solid-state NMR of Inorganic Materials, Pergamon, New York, 2002.

[25] N. Janes, E. Oldfield, J. Am. Chem. Soc. 107 (1985) 6769.

[26] G. Engelhardt, H. Koller, NMR – Basic Principles and Progress 31 (1997) 1.

[27] T. Nanba, M. Nishimura, Y. Miura, Geochim. Cosmochim. Acta 68 (24) (2004) 5103.

[28] B. Marler, A. Ertl, Am. Mineral. 87 (2002) 364.

[29] J.F. Stebbins, Nuclear magnetic resonance spectroscopy of silicates and oxides in geochemistry and geophysics, in: T.H. Ahrens (Ed.), Handbook of Physical Constants, American Geophysical Union, 1994.

[30] B.C. Bunker, R.J. Kirkpatrick, R.K. Brow, G.L. Turner, C. Nelson, J. Am. Ceram. Soc. 74 (6) (1991) 1430.

[31] L. Zuchner, J.C.C. Chan, W. Muller-Warmuth, H. Eckert, J. Phys. Chem. B 102 (23) (1998) 4495.

[32] L.S. Du, J.F. Stebbins, Solid State Nucl. Magn. Reson. 27 (2005) 37.

[33] S.K. Lee, J.F. Stebbins, J. Phys. Chem. B 104 (2000) 4091.

[34] M. Bertmer, L. Zuchner, J.C.C. Chan, H. Eckert, J. Phys. Chem. B 104 (28) (2000) 6541.

[35] M. Schmucker, K.J.D. MacKenzie, H. Schneider, R. Meinhold, J. Non-Cryst. Solids 217 (1997) 99.

[36] W.F. Du, K. Kuraoka, T. Akai, T. Yazawa, J. Mater. Sci. 35 (2000) 4865.

[37] D. Mao, P.J. Bray, Solid State Nucl. Magn. Reson. 1 (1992) 225.

[38] S. Sen, J.F. Stebbins, N.G. Hemming, B. Ghosh, Am. Mineral. 79 (9–10) (1994) 819.